

Effects of Pyrolysis Temperature on the Release Characteristics of Polycyclic Aromatic Hydrocarbons during Pyrolysis of Corn Stover Pellet

Lijie Li,^{a,b} Wenjuan Niu,^a Hongbin Cong,^b Haibo Meng,^{b,*} Zhiyou Niu,^{a,*} Xiuli Shen,^b Licong Cao,^b and Xianrui Kong^a

The release characteristics of polycyclic aromatic hydrocarbons during the pyrolysis of biomass remain poorly understood. This study investigated the effects of pyrolysis temperature on the polycyclic aromatic hydrocarbon release characteristics by analyzing both the transient vapor products and the physicochemical properties of corresponding biochar from the pyrolysis of corn stover pellets. The results revealed that the transient volatile compounds mainly included phenols, ketones, acids, furans, aldehydes, substances containing benzene ring, polycyclic aromatic compounds, and gaseous products. A range of 2 to 4 ring polycyclic aromatic hydrocarbons were generated at 400 to 700 °C with the peak at 560 °C, and the sum of relative content of polycyclic aromatic hydrocarbons ranged from 0.23% to 40.36%. For the biochar, the carbonization stage (400 to 700 °C) of corn stover pellets was further divided into three evolutionary stages, including the preliminary carbonization stage (380 to 480 °C), amorphous carbon structure stage (480 to 600 °C), and the stage of dehydrogenation and growth of aromatic rings (600 to 700 °C). The relationship between polycyclic aromatic hydrocarbon release in volatile compounds and H/C ratio of the biochar could be described by a power function.

DOI: 10.15376/biores.18.1.2112-2136

Keywords: Corn stover pellet; Pyrolysis; Pyrolysis temperature; Polycyclic aromatic hydrocarbons; Transient vapor products

Contact information: a: Key Laboratory of Agricultural Equipment in Mid-lower Yangtze River, Ministry of Agriculture, College of Engineering, Huazhong Agricultural University, Wuhan, Hubei 430070, P. R. China; b: Key Laboratory of Energy Resource Utilization from Agriculture Residue, Ministry of Agriculture and Rural Affairs, Academy of Agricultural Planning and Engineering, Beijing, 100125, P. R. China; *Corresponding author: newmh7209@163.com; nzhy@mail.hzau.edu.cn

INTRODUCTION

Renewable energy is of growing importance in addressing the environmental concerns over fossil fuel usage, as it has been widely promoted as an alternative to fossil fuel and a potential strategy to tackle climate changes at the global and national scales (IEA 2018). Energy from crop residues is considered as a form of renewable energy with low cost and rich reserves. Corn is a typical food crop widely planted in the world. Accordingly, a large quantity of corn stover is produced every year, and it is rich in cellulose, hemicellulose, and lignin (Han *et al.* 2021). The high carbon content (over 40%) in corn stover makes it a valuable resource of renewable and clean energy (Niu *et al.* 2016).

Pyrolysis is an advanced technology of thermal treatment. Pyrolysis of corn stover has received increasing attention and is regarded as an effective strategy to reduce the carbon dioxide concentration from the perspective of global carbon cycle (Yang *et al.* 2021). Moreover, the preparation of corn stover pellets can reduce the volume of accumulation and cost of transportation. In addition, the biochar derived from pelleted corn stover can alleviate dust emissions caused by biochar powder during entry into soils (Gelardi *et al.* 2019; Xie *et al.* 2021). However, the pyrolysis of biomass is generally accompanied by the production of polycyclic aromatic hydrocarbons (PAHs), which is mainly distributed in liquid bio-oil, accounting for 62% to 92.7% of the total PAHs (Fagernäs *et al.* 2012; Zhao *et al.* 2020), causing the risk of carrying PAHs for the biochar (Odinga *et al.* 2021) and gas products (Zhao *et al.* 2020). In this study, PAHs generally refer to the sixteen PAHs listed by US EPA (Zhou *et al.* 2014a).

As undesired components in the pyrolysis products, PAHs are carcinogenic and/or mutagenic. The presence of PAHs has a negative effect on the utilization of pyrolysis products. For example, PAHs in biochar are dangerous components for soil improvement, feed additives, or cooking (Lehmann *et al.* 2015; Wang *et al.* 2019). Many countries or organizations have set certain limits about PAHs in biochar, especially the International Biochar Initiative (IBI) and European Biochar Certificate (EBC). In addition, during the utilization of bio-oil in cogeneration unit, PAHs pose threats to the environment and the operator's health, and the presence of PAHs is not conducive to the upgrading of bio-oil (Stark and Ghoniem 2017).

For the pyrolysis-based poly-generation systems (Cong *et al.* 2018), the pyrolysis of biomass is expected to produce not only cleaner noncondensable gases, but also cleaner biochar. Although some studies have reported on the factors affecting the release of PAHs during biomass pyrolysis, such as the residence time of hot volatile compounds (Buss *et al.* 2016), biomass feedstock type (Krzyszczak *et al.* 2021; Zhou *et al.* 2014a), biomass particle size (Li *et al.* 2016; Stark and Ghoniem 2017), pyrolysis equipment (Weidemann *et al.* 2018), and catalysts (Cho *et al.* 2020; Muneer *et al.* 2019), they have only focused on the engineering conditions of pyrolysis, while the formation and release mechanisms of PAHs based on pyrolysis process have been largely ignored. Furthermore, many studies have indicated the presence of PAHs in the biochar mainly for the following reasons. The formation of biochar skeleton structure produces PAHs in the biochar, and the PAHs in the tar are adhered to the surface and pore of the biochar, which also contributes to the accumulation of PAHs (Fagernäs *et al.* 2012; Lehmann *et al.* 2015; Zhao *et al.* 2020). Therefore, understanding the formation and distribution mechanisms of PAHs during the pyrolysis of biomass will help to take more targeted measures to inhibit the formation of PAHs in the pyrolysis products. However, little is known about the release characteristics of PAHs at different temperatures during the pyrolysis process. Furthermore, the relationship between the release amount of PAHs in the volatile compounds from the pyrolysis of biomass and the aromaticity of biochar remains poorly understood.

Previous studies of PAHs in biomass pyrolysis products mostly adopted tubular furnace, batch pyrolysis reactor, and continuous pyrolysis reactor (Buss *et al.* 2016; Zhao *et al.* 2020). Due to the limitations of experimental equipment architecture and gas flow characteristics, volatile components could not leave the reaction system quickly, resulting in the secondary reaction of the volatile components (Legarra *et al.* 2019). Therefore, the obtained PAHs were produced under the combined action of primary reaction and secondary reaction, which largely hinders the dissection of the specific PAH formation mechanism, particularly during the primary reaction. The main reason is that it is extremely

difficult to quickly remove the volatile components from the reaction system. In addition, bio-oil aging also makes it difficult to obtain primary products (Wang and Ben 2020). Therefore, a special design of the experimental equipment is highly necessary.

In this study, a thermogravimetric analyzer coupled with gas chromatography and mass spectrometry system (TG–GC/MS) was specially assembled to investigate the release characteristics of PAHs during pyrolysis process of corn stover pellets. The species and relative contents of volatile components, especially PAHs from the pyrolyzate plume, were semi-quantitatively analyzed during the pyrolysis process of corn stover pellets from 200 to 700 °C, and the physicochemical characteristics of biochar produced were analyzed in the pyrolysis process. The formation and evolution mechanisms of PAHs in the transient vapor products was investigated, as well as the relationship between the release amount of PAHs and the aromaticity of biochar during the pyrolysis of corn stover pellets.

EXPERIMENTAL

Materials

Sample collection and preparation

Corn stover (CS) was collected from Harbin, Heilongjiang province, China. It was ground by a FQ–320 grinder (FQ–320, Zhengzhou Yunkai mechanical equipment Co., Ltd, Zhengzhou, China) after natural drying, followed by oven drying at 105 °C for 12 h until it reached a constant mass. The milled corn stover was collected, and 293.78 ± 2.31 mg of milled corn stover sample was held for 5 s at 8 MPa and pressed into pellets (diameter 13 mm, height 1.1 mm) by tablet press. The corn stover pellet samples and tablets were stored in a drying dish.

Methods

Proximate and ultimate compositions

Proximate analysis of corn stover pellets was conducted according to ASTM D3302/D3302M (2015), ASTM 3174(2012), and ASTM3175(2011) (1984). The ash content of the biochar was determined with a thermogravimetric analyzer (TG STA449Fs, NETZSCH, Selb, Germany). Ultimate analysis of biochar was conducted by an elemental analyzer (Vario EL III, Elementar, Langensfeld, Germany) to determine the C, H, N, and S contents. The O content was obtained by subtracting the C, H, N, S, and ash contents from 100%. The results are shown in Table 1.

Determination of cellulose, hemicellulose, and lignin

Cellulose, hemicellulose, and lignin in the corn stover pellets were determined by the Van Soest's washing fiber analysis method according to NY/T 3494 (2019).

TG–FTIR- MS

The pyrolysis vapor on-line analysis of the samples was carried out by using a synchronous thermal analyzer (SDT Q600, TA Instruments, Newcastle, DE, USA), a Fourier transform infrared spectrometer (Nicolet i50, Thermo Fisher, Waltham, MA, USA), and a fast process mass spectrometry (MS, AMETEK, Philadelphia, PA, USA). The bio-crudes were detected by a Fourier transform infrared spectrometer, while a fast process mass spectrometry was employed to analyze the gaseous products (CO, CH₄, H₂, and C₂H₂). The test conditions were as follows: the carrier gas was 99.999% high-purity

nitrogen, and the gas flow rate was 100 mL/min. The heating rate was 20 °C/min, and the temperature was from 25 to 900 °C. The temperature of the transfer tube and detector was 220 °C, and the scanning range was 4000 to 400 cm⁻¹.

TG–GC/MS

Pyrolysis experiments were performed on the thermogravimetric analyzer (TG STA449Fs, NETZSCH, Selb, Germany) coupled with gas chromatography–mass spectrometry (GC 7890B and MS 5977B, Agilent, Hercules, CA, USA), and the schematic diagram of the TG–GC/MS reaction system is shown in Fig. 1. The reaction temperature was set to 250, 280, 320, 380, 400, 440, 480, 500, 520, 560, 600, 660, and 700 °C, respectively. The temperature of the pyrolysis vapor products transfer tube was kept at 295 °C to prevent product condensation. About 1 mL of high temperature (300 °C) volatile sample was picked by the loop in the high temperature injection valve, carried by helium gas into GC, and then detected by mass spectrometry. It took about 0.5 s for the detection of the products after being released in an oxygen free environment. Therefore, the pyrolysis vapor products were instantly sampled and analyzed once generated to minimize the potential contribution of secondary gas phase reactions to the formation of PAHs. The heated furnace was continuously purged with a 100 mL/min helium gas flow. When the aim temperature was reached, the pyrolysis vapor from the reactor of the thermogravimetric analyzer was extracted by a peristaltic pump and carried by helium gas through a stainless steel pipe (inner diameter 0.75 mm, with passivated inner surface). The biochar from every test was designated as CS200, CS250, CS280, CS320, CS380, CS400, CS440, CS480, CS500, CS520, CS560, CS600, CS660, and CS700, respectively.

The GC/MS was fitted with a 30 m × 250 μm × 0.25 μm HP–5MS UI equivalent column. The GC oven was initially heated at 40 °C for 1 min, and the temperature was subsequently increased to 100 °C at 1.5 °C/min and held for 2 min, increased to 150 °C at a rate of 5 °C/min and held for 1 min, increased to 230 °C at a rate of 20 °C/min and held for 1 min, and then increased to 310 °C at a rate of 20 °C/min and held for 5 min (total analysis time of 68 min). The manifold was at 320 °C and the ion trap temperature was held at 300 °C. The GC/MS results were compared with the NIST 17 database.

The 16 mixed standard PAHs dissolved in hexane used for calibration were purchased from TanMo Quality Testing Technology Co., Ltd. (Beijing, China). PAHs in the products were pre-calibrated by injection of the 16 mixed standard PAHs dissolved in hexane. The GC/MS analysis spectra of US EPA 16PAHs are shown in Fig. S1, and their retention time is shown in Table S1. The product components were semi-quantified based on ratio of peak area of the target substance to the initial mass of loaded sample.

$$I_i = \frac{A_i}{m_0} \quad (1)$$

$$\eta = \frac{A_i}{A_T} \quad (2)$$

In the equations, I_i represents the ratio of peak area of the target substance to the initial mass, namely, the absolute yield, mg⁻¹; A_i represents the peak area of the target substance, dimensionless; A_T represents the sum of peak areas of all released compounds, dimensionless; and m_0 represents the initial mass of the loaded sample, mg.

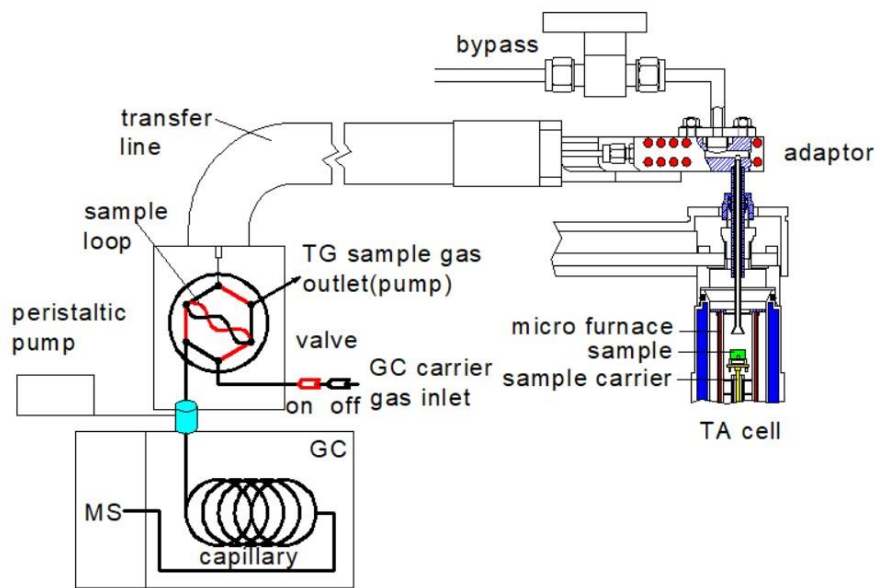


Fig. 1. Schematic diagram of the TG-GC/MS reaction system

FTIR analysis

Biochar mentioned in this paper refers to the residue generated by pyrolysis of corn straw pellets at different temperatures on TG-GC/MS. The surface functional groups of crop residue and biochar were detected by using FTIR. The sample was mixed with KBr at the ratio of 1:100 and then made into tablets before scanning with an FTIR spectrometer.

Raman analysis

The structural features of biochar were characterized by Raman spectroscopy (Renishaw inVia Raman microscope, London, UK) with a laser at a wavelength of 785 nm. Detailed parameters are shown in the Supplementary Information. Raman spectra of the biochar were fitted by using 10 bands according to the method proposed by Li *et al.* (2006). The D band was assigned to C-C between aromatic rings and aromatics with not less than 6 rings, and the G_R , V_L , and V_R bands were assigned to aromatics with 3 to 5 rings and amorphous carbon structures. The band area ratio was taken as a brief measure of the ratio between the large aromatic ring systems and the aromatic ring systems typically found in amorphous carbon (Li *et al.* 2006).

$$I_D / I_{(G_R+V_L+V_R)} = \frac{S_D}{S_{(G_R+V_L+V_R)}} \quad (3)$$

In Eq. 3, S_D means the area of the D band, and $S_{(G_R+V_L+V_R)}$ represents the total area of the G_R , V_L , and V_R bands.

RESULTS AND DISCUSSION

Characteristics of corn stover

Composition and higher heating value (HHV) of corn stover pellets are shown in Table 1. The main components of corn stover pellets are cellulose, hemicellulose, and

lignin, of which the content of cellulose is the highest, up to $39.32 \pm 0.94\%$. The results of approximate analysis show that volatile matter was much greater than ash and fixed carbon. The results of elemental analysis showed that C was the most abundant element, followed by O.

Table 1. Composition and Higher Heating Value (HHV) of Corn Stover Pellets

Parameters	Value
Cellulose (% dry basis)	39.32 ± 0.94
Lignin (% dry basis)	10.16 ± 0.31
Hemicellulose (% dry basis)	29.93 ± 0.82
Volatile matter (% dry basis)	76.53 ± 0.03
Fixed carbon ^a (% dry basis)	15.54 ± 0.11
Ash (% dry basis)	7.91 ± 0.08
C (% dry basis)	44.52 ± 0.24
H (% dry basis)	5.74 ± 0.07
O ^a (% dry basis)	38.71 ± 0.32
N (% dry basis)	2.93 ± 0.1
S (% dry basis)	0.57 ± 0.04
HHV (MJ/kg dry basis)	17.44 ± 1.53
^a Acquired by subtraction	

TG-FTIR-MS Analysis of the Pyrolysis of Corn Stover Pellets

The TG/DTG curves of the pyrolysis of corn stover pellets and the FTIR analysis results of pyrolysis volatile compounds are shown in Fig. 2. The weight loss process of corn stover pellets can be divided into three stages. These are: (1) a drying stage, at which the evaporation of water resulted in a slight weight loss; (2) a volatile matter escaping stage, at which the main released substances were water, carbon dioxide and acetic acid before $250\text{ }^{\circ}\text{C}$ (Fig. 2b); and (3), a carbonization stage. During the second stage, the cellulose, hemicellulose, and lignin in the corn stover pellets were gradually decomposed, resulting in the release of small molecular substances and formation of volatile components, including acetic acid, alkanes, and furans (Fig. 2b). The maximum weight loss rate of corn stover pellet was obtained (Fig. 2a), and the total absorbance of volatile compounds was the highest at $320\text{ }^{\circ}\text{C}$. With increasing pyrolysis temperature, the total absorbance of volatile compounds at different temperatures after $320\text{ }^{\circ}\text{C}$ decreased. The volatile compounds released from the pyrolysis mainly included CO_2 (2390 to 2280 cm^{-1}), CO (2173 to 2120 cm^{-1}), CH_4 (2960 cm^{-1}), and alkanes (2928 cm^{-1}). The easily condensable substances included H_2O (3357 cm^{-1}), carbonyl compounds $\text{C}=\text{O}$ (1760 to 1660 cm^{-1}), furans (1240 to 1160 cm^{-1}), and acid RCOOH (1300 to 1200 cm^{-1}). The carbonyl $\text{C}=\text{O}$ stretching signal was the strongest, and the DTG curve formed the maximum peak at this stage (Fig. 2a). The main reason might be that cellulose and hemicellulose were decomposed at 250 to $440\text{ }^{\circ}\text{C}$ and 250 to $400\text{ }^{\circ}\text{C}$, respectively, and lignin was decomposed at 200 to $500\text{ }^{\circ}\text{C}$, accompanied by a series of dehydrogenation and decarboxylation reactions (Liu *et al.* 2019). In the carbonization stage, the aromatic rings in the biochar were further condensed and the side chains were broken, accompanied by a slight weight loss and the release of a relatively high amount of H_2 .

The composition of main non-condensable gases during corn stover pellet pyrolysis was detected (Figs. 2b, 2c). The highest peaks of CO and CO_2 release were observed at $320\text{ }^{\circ}\text{C}$, the temperature corresponding to the maximum weight loss. The release of CO_2 could be ascribed to the cracking of functional groups of carboxyl ($\text{C}=\text{O}$) and COOH

during the pyrolysis process. CH_4 was released at below $300\text{ }^\circ\text{C}$ and reached peaks at $380\text{ }^\circ\text{C}$ and $560\text{ }^\circ\text{C}$, respectively (Figs. 2b, 2c). CH_4 was generated through the decomposition of methoxyl mainly from hemicellulose, cellulose, and lignin in corn stover pellets, and lignin had the highest methoxyl content (Yang *et al.* 2020a). A small amount of C_2H_2 was released from $400\text{ }^\circ\text{C}$ to $600\text{ }^\circ\text{C}$ (Fig. 2c). The production of C_2H_2 was due to the decomposition of C_2H_4 and certain aromatic tar components (Font Palma 2013). A small amount of H_2 was produced between 300 and $600\text{ }^\circ\text{C}$, and the production increased rapidly after $600\text{ }^\circ\text{C}$. The production of H_2 could be attributed to the dehydrogenation polymerization of aromatic rings (Yang *et al.* 2020b).

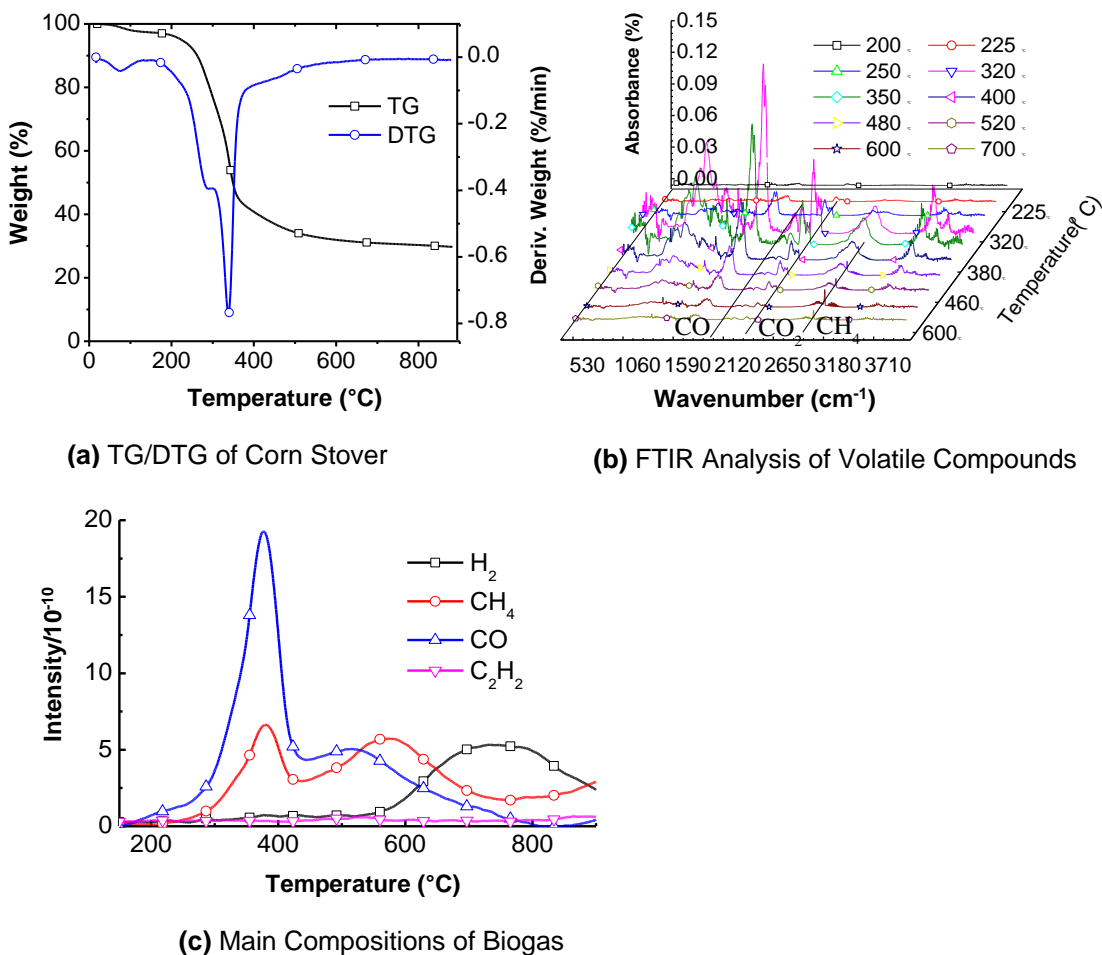


Fig. 2. TG/DTG curves (a), FTIR analysis of volatile compounds (b) and the main gas composition (c) during the pyrolysis of corn stover pellets

TG-GC/MS of the Pyrolysis of Corn Stover Pellets

The overall product distribution during the pyrolysis of corn stover pellet at different temperatures is presented in Fig. 3. Volatile compounds were mainly released at 250 to $700\text{ }^\circ\text{C}$ during the pyrolysis process of corn stover. Acids, aldehydes, ketones, and phenols were mainly generated at the early stage of the pyrolysis. The acids appeared at the temperature between 250 and $400\text{ }^\circ\text{C}$, including acetic acid and a small amount of formic acid and propionic acid. The ketones were mainly generated in the temperature range between 250 and $500\text{ }^\circ\text{C}$, including acetone, 1-hydroxy-2-propanone, and 2-cyclopenten-1-one. Furans were released from 250 to $480\text{ }^\circ\text{C}$, including 3-furaldehyde and

dibenzofuran. Phenols were produced at 250 to 600 °C, including phenol, 5-ethenyl-2-methoxy-phenol, 2-methoxy-phenol, 2-methoxy-phenol, catechol, and p-cresol. Benzenes and polycyclic aromatic compounds (PACs) were generated in the later pyrolysis stage. Benzenes were produced at the temperature from 250 to 700 °C, including benzene, homologues of benzene, and some other substances containing benzene ring (except for benzofuran, phenol, and PACs). PACs were produced at temperatures from 380 to 700 °C, including eight PAHs, a large number of derivatives of naphthalene, fluorine, phenanthrene, and a few derivatives of anthracene and pyrene. The formation of PACs occurred in the period during which the weight loss of the corn stover pellets increased from 59.3% to 69.2% (Fig. 3a), and the relative content of PACs reached 47.2% at 600 °C (Fig. 3b). In addition to the volatile compounds described above, sugars, short chain hydrocarbons, pyrrole, and indole were also produced during the pyrolysis process of corn stover pellets.

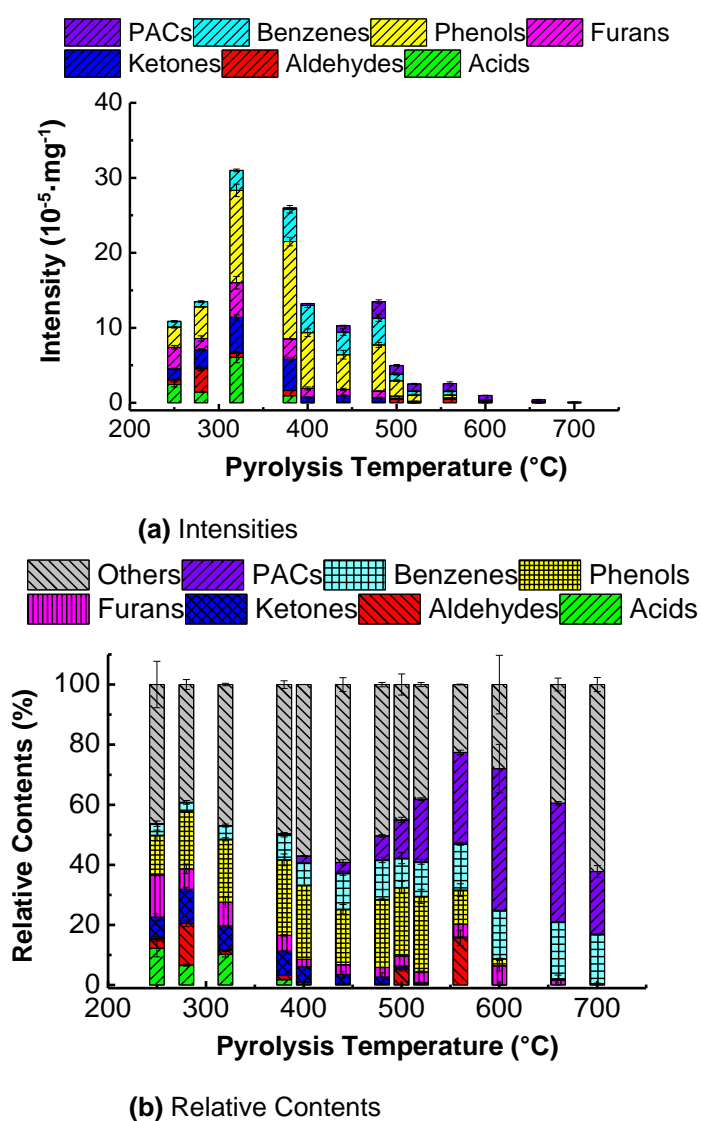


Fig. 3. Distribution of transient volatile compounds of corn stover pellets during pyrolysis at different temperatures

The release intensity of phenols reached the maximum at the temperature between 320 and 380 °C, followed by rapid decreases, while that of PACs began to increase from 380 to 480 °C (Fig. 3a). The release intensity of phenols and PACs showed opposite trends in the same temperature range of 380 to 600 °C (Fig. 3a), indicating that the production of PAHs might be attributed to the deep decomposition of lignin structure (Zhou *et al.* 2014). Previous studies reported that PACs were detected at 350 °C (Lee *et al.* 2008; Zhao *et al.* 2020), and the volatile compounds from biomass in the tube furnace might stay in the reactor for a certain time, between half an hour and 2 hours generally (Li *et al.* 2016; Zhao *et al.* 2020). However, in this study, the reason for the detection of PACs at higher temperature may be that biochar did stay not longer than about 1 minute at any temperature due to the relatively sufficient carrier gas flow. The volatile compounds might be quickly removed by the peristaltic pump used in this study, resulting in a very short residence time, which would minimize the secondary reaction of volatile compounds so as to inhibit the formation of PAHs (Wong *et al.* 2019).

Effects of Pyrolysis Temperature on PAH Monomer and Homologues

PAH monomer

Figure 4 shows the total amounts of generated PAHs in the volatile compounds from the pyrolysis of corn stover pellets at different temperatures. With the increase of temperature from 400 to 700 °C, the release intensity of PAHs firstly increased and then decreased. These PAHs contained a series of 2 to 4 ring compounds, including naphthalene, acenaphthylene, acenaphthene, fluorene, phenanthrene, fluoranthene, and pyrene. Naphthalene, phenanthrene and fluorene were the major contributors to the release intensity and relative content of total PAHs, followed by anthracene, acenaphthylene, acenaphthene, fluoranthene, and pyrene. At 400 °C, fluorene was the most abundant PAH (up to 0.35 %), and naphthalene was always the most abundant PAH (up to 32.90 %) in the transient volatile compounds between 440 and 700 °C. The relative content of 3-ring PAHs reached up to 15.22 % at 600 °C, and that of 4-ring PAHs was lower than 0.2 % before 560 °C and became 0.27 % at 600 °C. High temperature is more beneficial for the formation and release of middle-molecular-weight components (Zhao *et al.* 2020). These observations are also in accordance with the evolution profiles of PAHs from McGrath *et al.* (2007), in which the PAHs in tar reached the highest value at the temperature between 500 and 550 °C, and then decreased sharply (McGrath *et al.* 2007).

With the pyrolysis temperature increasing from 520 to 560 °C, the relative content of PAHs rose rapidly from 6.15% to 16.36% (Fig. 4), and then the release intensity of PAHs reached the highest at 560 °C. With further increases of temperature, the relative content of PAHs reached the peak at 600 to 660 °C. Therefore, considering the release of PAHs, 560 °C could be a landmark temperature for the pyrolysis process of corn stover. The production of bio-oil at temperatures lower than 560 °C may be conducive to the further upgrading and transformation of the bio-oil. Therefore, the discovery of this temperature explains the optimization mechanism of bio-oil.

In previous studies, PAHs with larger ring sizes were detected (Xiong *et al.* 2020; Zhao *et al.* 2020), but they were not detected in this study, which does not mean that they were not produced. No detection of such PAHs may be related to the vapor pressure of the PAHs with larger ring sizes and the limitation of online monitoring (Tsekos *et al.* 2020).

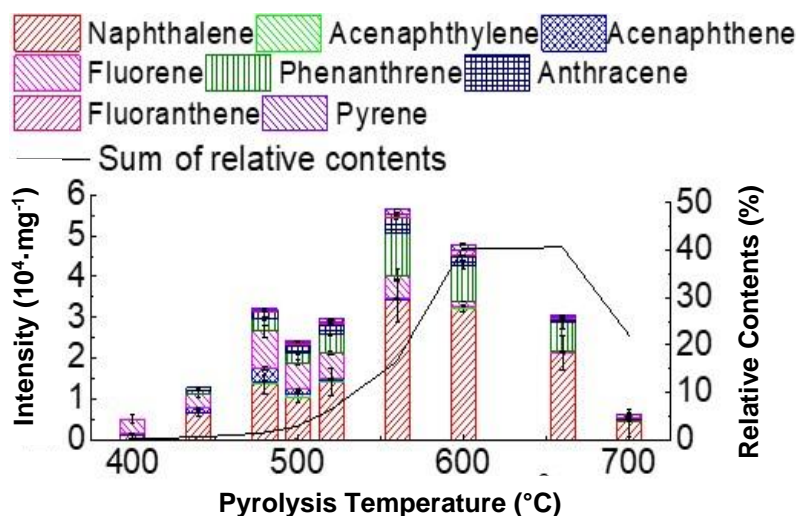
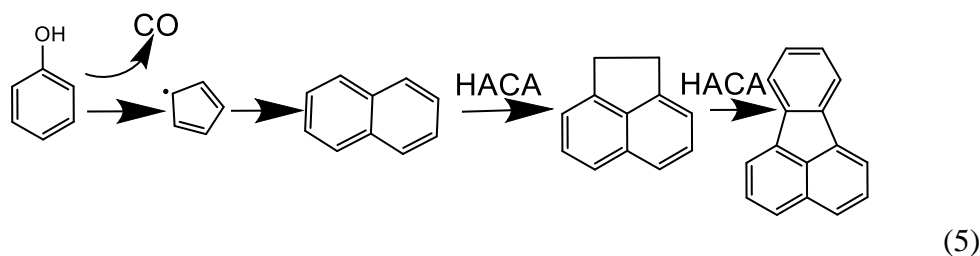
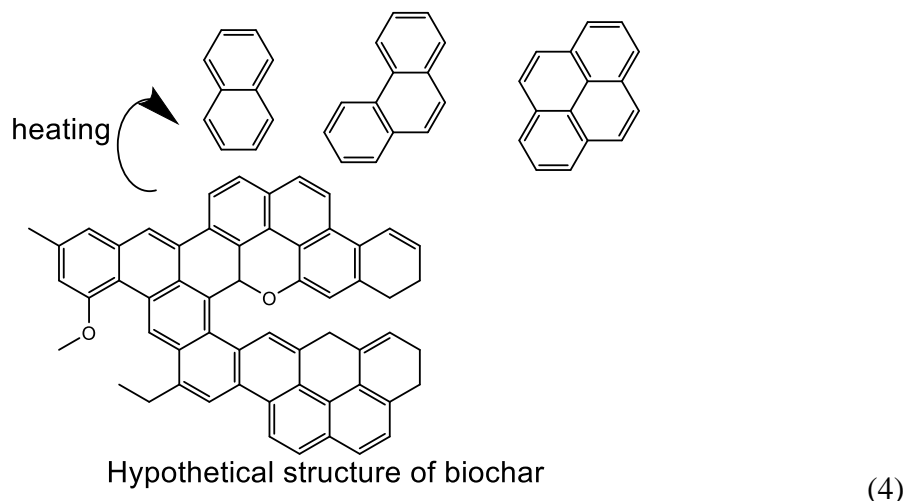


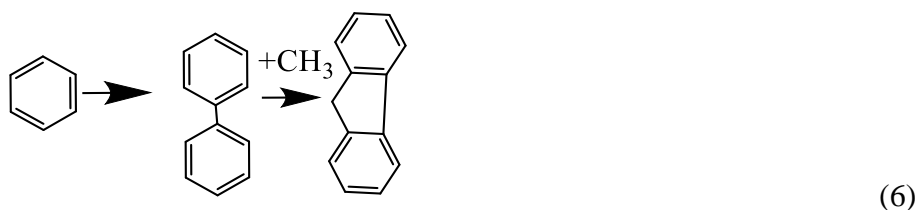
Fig. 4. Total amount of the generated PAHs during the pyrolysis of corn stover pellets

The evolution of PAHs in volatile compounds with pyrolysis temperature during pyrolysis of corn stover pellets is shown in Fig. 5. The evolutionary profiles of each PAH monomer were different along with temperature. The temperature for the peak production of these eight PAHs followed the order of acenaphthene (480 °C), fluorene (480 °C), acenaphthylene (500 °C), naphthalene (560 °C), phenanthrene (560 °C), anthracene (560 °C), fluoranthene (600 °C), and pyrene (600 °C). Acenaphthene was the first species to disappear, and a small amount of other species were released until 700 °C (Figs. 5a-h). Acenaphthylene, acenaphthene, and fluorene were mainly produced at relatively lower temperature, and five other species were produced at relatively higher temperature (Fig. 5). With the increase in pyrolysis temperature, the release of 2-ring PAHs decreased and that of 3-ring and 4-ring PAHs increased, which may be related to the different formation mechanism of each PAH monomer.

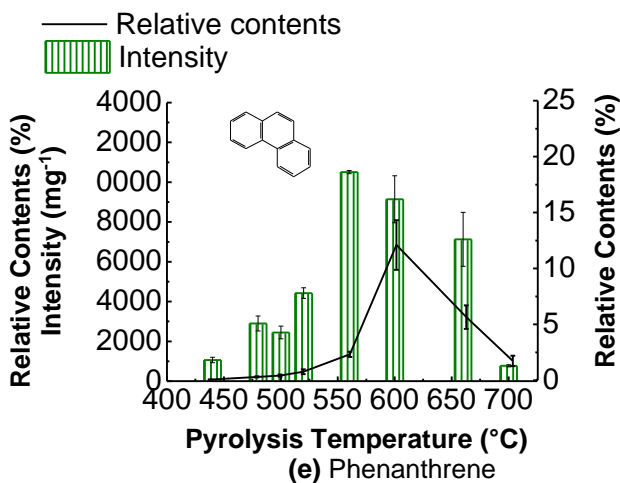
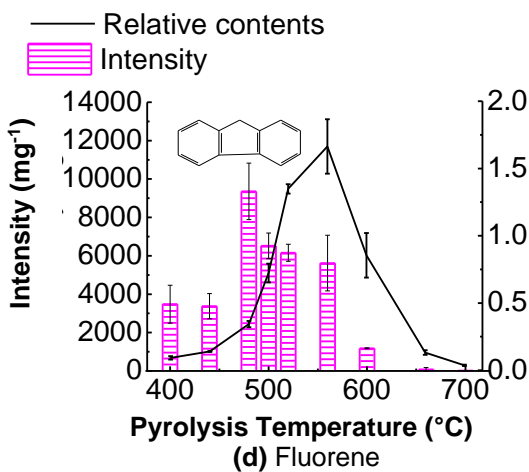
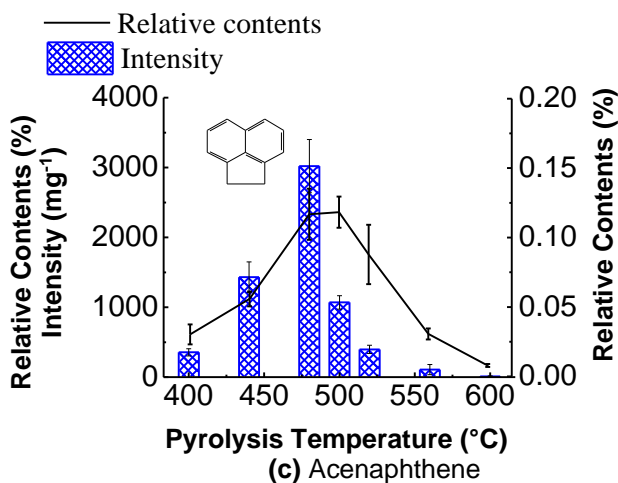
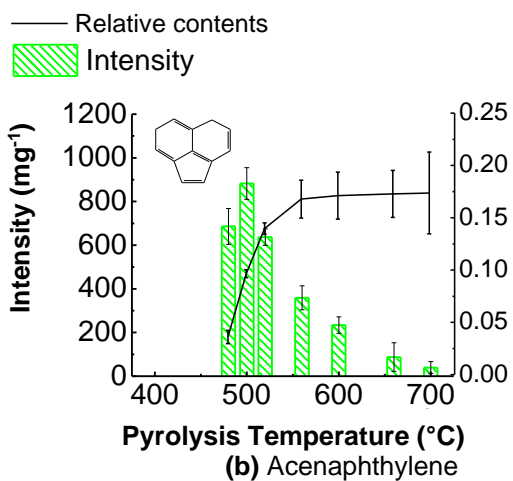
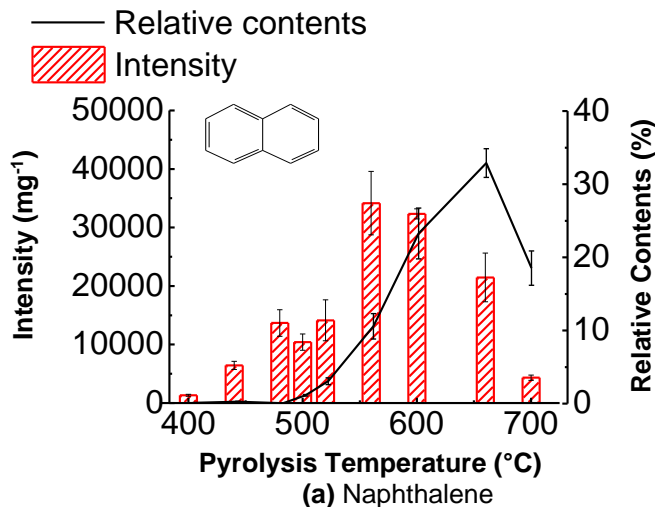
The release intensity peak of naphthalene appeared at 560 °C. The relative content of naphthalene rapidly increased from with increasing temperature from 400 to 660 °C, and then it decreased to 0.11% with further increases in temperature from 660 to 700 °C (Fig. 5a). Two possible ways may be used to explain naphthalene formation. In the first pathway, naphthalene was primarily evaporated from biochar according to low temperature PAH formation mechanism (Eq. 4) (McGrath *et al.* 2007; Friederici *et al.* 2021). In the second pathway, phenol as a PAH precursor was transformed to cyclopentadiene, and naphthalene was formed from the cyclopentadienyl radicals (Sharma and Hajaligol 2003). However, the decrease in naphthalene may be due to the formation of fluoranthene and anthracene after 660 °C (Eq. 5) (Zhou *et al.* 2015). Acenaphthene just appeared at the temperature between 400 and 600 °C, and the release intensity dropped rapidly after 480 °C (Fig. 5c). However, acenaphthylene began to be produced at 480 °C, and its release decreased with increasing temperature after 500 °C (Fig. 5d). In view of the emergence of acetylene at 400 to 600 °C (Fig. 2c), it could be inferred that acenaphthene might come from hydrogen abstraction acetylene addition (HACA) pathway (Eq. 5). The reduction of acenaphthene release suggested that acenaphthene might be an intermediate for the formation of other PAHs. For example, acenaphthylene could be obtained by dehydrogenation and fluoranthene could be obtained by acetylene addition (Liu *et al.* 2017).



The release intensity of phenanthrene and anthracene was similar within the same temperature range. Their release intensity increased from 440 to 560 °C, reached the maximum at 560 °C, and decreased from 600 to 700 °C. Their relative content reached the maximum at 600 °C, which was 12.10% and 2.09%, respectively. Fluorene began to be produced at 400 °C, and it reached a maximum at 480 °C, followed by gradual decreases (Fig. 5e). The formation of fluorene may be due to the addition of biphenyl and methyl radical (Eq. 6), and previous studies have suggested that lignin could produce higher concentrations of fluorine (Zhou *et al.* 2015).



The release profiles of fluoranthene and pyrene were similar, both of which were produced at 480 °C (Figs. 5f–g), increased slowly from 480 to 600 °C, and then reached a maximum at 600 °C (Figs. 5f–g). Considering that fluoranthene and pyrene were mainly produced at high temperature, they might be mainly evaporated from biochar. Another possible formation path of acenaphthylene, acenaphthene and fluorene may be that they were formed during the solid-phase charring process (Lee *et al.* 2008), because their methyl substitutes were also not detected in the volatile components.



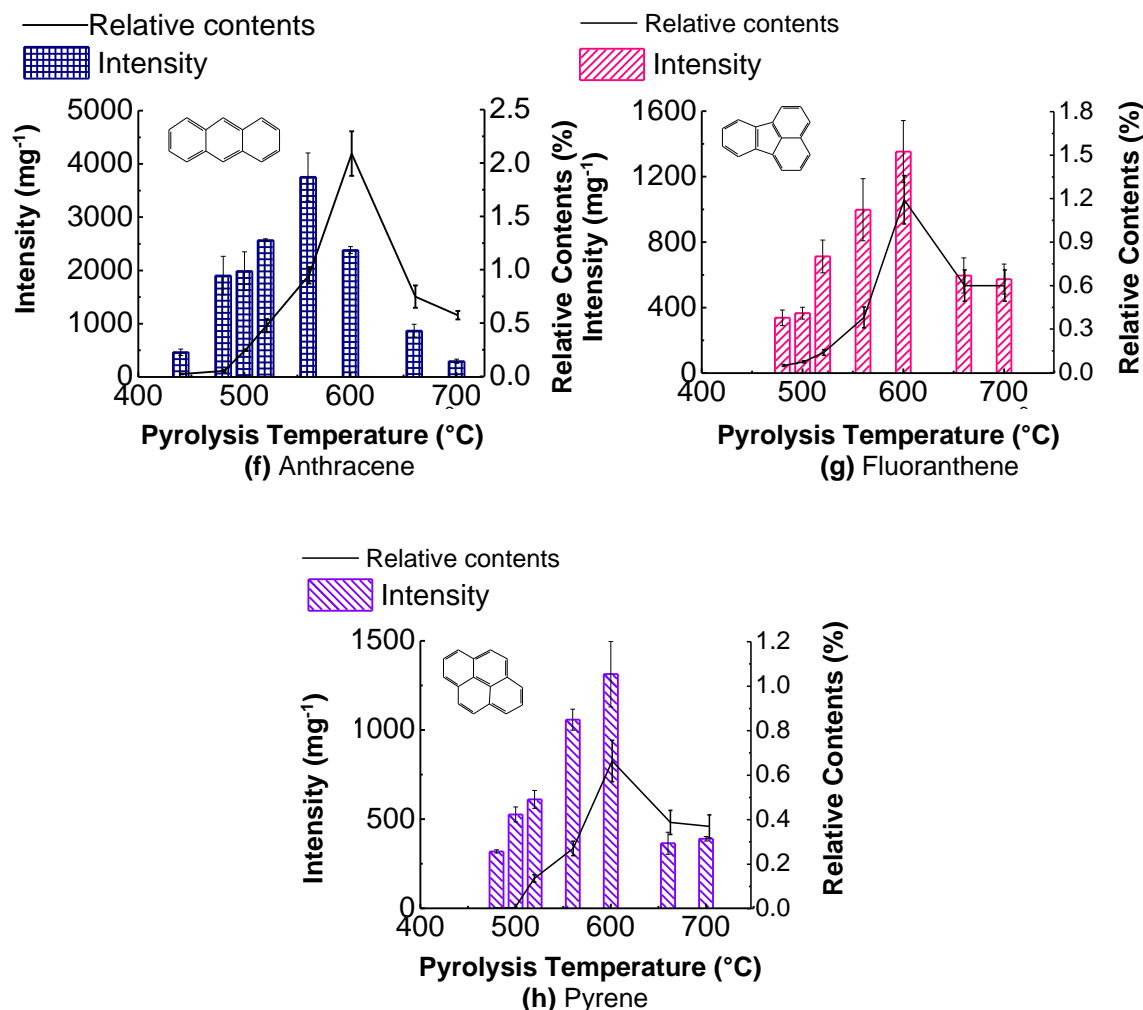
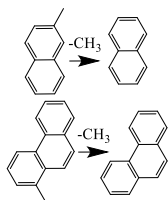


Fig. 5. Temperature evolution of PAHs in volatile compounds of corn stover pellets in pyrolysis

Effects of pyrolysis temperature on PAH homologues

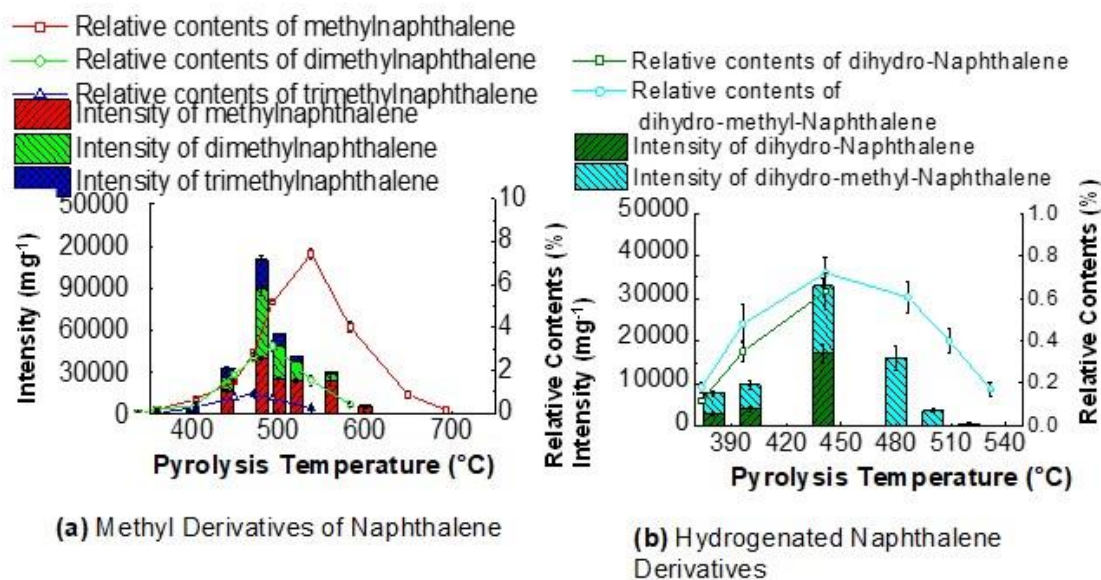
The related alkylated and hydrogenated PAHs were also determined, as a way to gain additional insights into the formation mechanisms and pathways of PAHs. Figure 6 shows the relative contents of naphthalene and phenanthrene homologues during the pyrolysis of corn stover pellets at different temperature. The 1-methylnaphthalene and 2-methylnaphthalene both increased at the temperature from 380 to 480 $^{\circ}\text{C}$, and then they decreased afterwards (Fig. 6a), which is consistent with the results of Zhou *et al.* (2015). The results indicate that methylnaphthalene may be converted into naphthalene through demethylation (Eq. 7). The dimethyl-substituted naphthalene contained ortho and meta isomers, all of which first increased from 400 $^{\circ}\text{C}$, reached the highest value at 480 $^{\circ}\text{C}$, and then decreased until 600 $^{\circ}\text{C}$ (Fig. 6a). The trimethyl naphthalene included 3 isomers, all of which first increased from 400 $^{\circ}\text{C}$, reached the peak at 480 $^{\circ}\text{C}$, and then decreased until 560 $^{\circ}\text{C}$ (Fig. 6a). The production of polymethyl-substituted naphthalene was because the substitution sites of naphthalene are more active, and the H atom is easily replaced by methyl. 1,2-dihydro-naphthalene and 1,2-dihydro-4-methyl-naphthalene were detected at 380 $^{\circ}\text{C}$, and disappeared at 440 and 520 $^{\circ}\text{C}$, respectively (Fig. 6b). Derivatives of fluorene were 9-methyl-9H-fluorene from 400 to 600 $^{\circ}\text{C}$ and 9,9-methyl-9H-fluorene from 400 to 560 $^{\circ}\text{C}$ (Fig. 6c), which might be attributed to the activation of biphenyl after being

attacked by methyl radical. The methyl substituents of phenanthrene mainly included methyl phenanthrene between 400 and 600 °C and dimethyl phenanthrene between 500 and 560 °C (Fig. 6d).



(7)

It is interesting to note that a large number of derivatives of naphthalene, fluorine, and phenanthrene, as well as a small amount of derivatives of acenaphthylene, acenaphthene, and fluoranthene were detected. However, the homologues and derivatives of acenaphthylene, acenaphthene, and fluoranthene were not detected. The peak of PAH derivatives released from corn stover pellet pyrolysis vapors appeared before that of corresponding PAH monomers (Figs. 5 and 6), which may be ascribed to methyl cracking at higher temperature. The methyl substituents of PAHs may be the precursor of PAHs (Liu *et al.* 2017). In addition, a small amount of oxy-PAHs have been found in the pyrolysis vapors, such as 1-naphthalenol, 5,8-dihydro-1-naphthalenol, and other homologues, but when the pyrolysis temperature was higher than 500 °C, they were not detected.



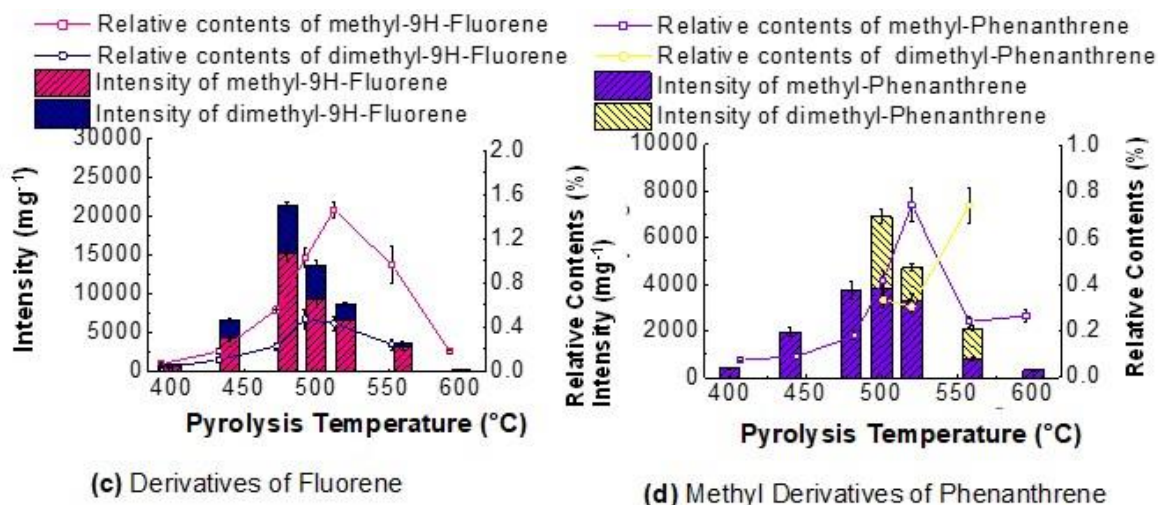


Fig. 6. Release intensities and relative contents of alkylated and hydrogenated PAHs of corn stover pellets during pyrolysis at different temperature

FTIR and Raman Analysis of the Biochar

The FTIR spectra of corn stover pellets and the biochar (CS200–CS700) are shown in Fig. 7. With increasing pyrolysis temperature, the peaks at 1100 to 1000 cm^{-1} were assigned to the hydroxyl group C-OH representing cellulose and hemicellulose (Yang *et al.* 2020b,c) of corn stover, which decreased gradually from 200 $^{\circ}\text{C}$, and totally disappeared at 300 $^{\circ}\text{C}$. However, the peak intensity of C=C ring stretching vibration (1514 cm^{-1}) representing lignin decreased until 400 $^{\circ}\text{C}$ (Chen *et al.* 2008). These phenomena indicated that the structure of cellulose and hemicellulose in corn stover was decomposed before 300 $^{\circ}\text{C}$ and the lignin structure was decomposed before 400 $^{\circ}\text{C}$ (Fig. 7). These results are consistent with previous studies of the three components (Yang *et al.* 2020a,b,c). The absorption peak at 1452 cm^{-1} can be ascribed to O-CH_3 of lignin, and the peak of O-CH_3 decreased gradually accompanied by the release of CH_4 (Yan *et al.* 2007). The bands of the aromatic =C-H out-of-plane (860 to 670 cm^{-1}) appeared from 400 $^{\circ}\text{C}$. The CH out-of-plane swing (2927, 2860, and 1380 cm^{-1}) disappeared in the biochar prepared after 480 $^{\circ}\text{C}$, indicating the disappearance of aliphatic CH_2 and enhancement of aromaticity. Meanwhile, the relative content of PAHs in the transient volatile components increased from 400 to 480 $^{\circ}\text{C}$ (Fig. 3), indicating that the release of PAHs is related to the aromaticity of the biochar.

Raman analysis can indicate the effect of heat treatment on the framework structure evolution of biochar (Sheng 2007). With increasing temperature, biomass is subjected to a series of decomposition reactions such as dehydrogenation and decarboxylation, and the aromatization would occur (Brewer *et al.* 2009; McGrath *et al.* 2007; Yang *et al.* 2020; Zhang *et al.* 2020). Raman spectra of the biochar derived from the pyrolysis of corn stover pellets are shown in Fig. 7b. The $I_D/I_{(G_R+V_L+V_R)}$ was stable at around 0.13 in the temperature range of 380 to 440 $^{\circ}\text{C}$, constant at around 0.23 in the temperature range of 480 to 520 $^{\circ}\text{C}$, decreased to 0.21 at 560 $^{\circ}\text{C}$, and increased gradually from 0.37 at 600 $^{\circ}\text{C}$ to 0.5 at 700 $^{\circ}\text{C}$. The changing trend of $I_D/I_{(G_R+V_L+V_R)}$ with pyrolysis temperature showed that the biochar derived from corn stover pellets underwent three evolutionary stages during the

carbonization stage of pyrolysis: (1) Stage of preliminary carbonization of residual solids (380 to 480 °C), at which cellulose, hemicellulose, and lignin of corn stover pellet were completely decomposed, and at the same time, derivatives of PAHs, phenols and benzene-containing substances were mainly released; (2) Stage of amorphous carbon structure (480 to 600 °C), at which the carbon structure was small aromatic ring systems with 3 to 5 fused benzene rings in the biochar and PAHs were the main components in the release, and 4-ring was the largest size; and (3) Stage of dehydrogenation and the growth of aromatic rings (600 to 700 °C), at which a larger aromatic system was developed (Li *et al.* 2006; Keiluweit *et al.* 2010; Zhao *et al.* 2016; Xiong *et al.* 2019). During the carbonization stage, the relative contents of phenanthrene, anthracene, fluoranthene, and pyrene reached the maximum, and the PAHs with larger rings (3, 4-ring) took a larger proportion. Combined with the highest release intensity of PAHs at 560 °C (Fig. 4), the relatively abundant amorphous carbon at around 560 °C at the second stage contributed to the release of PAHs (Fig. 7), indicating that there were relatively abundant free PAHs in the stage of amorphous carbon structure.

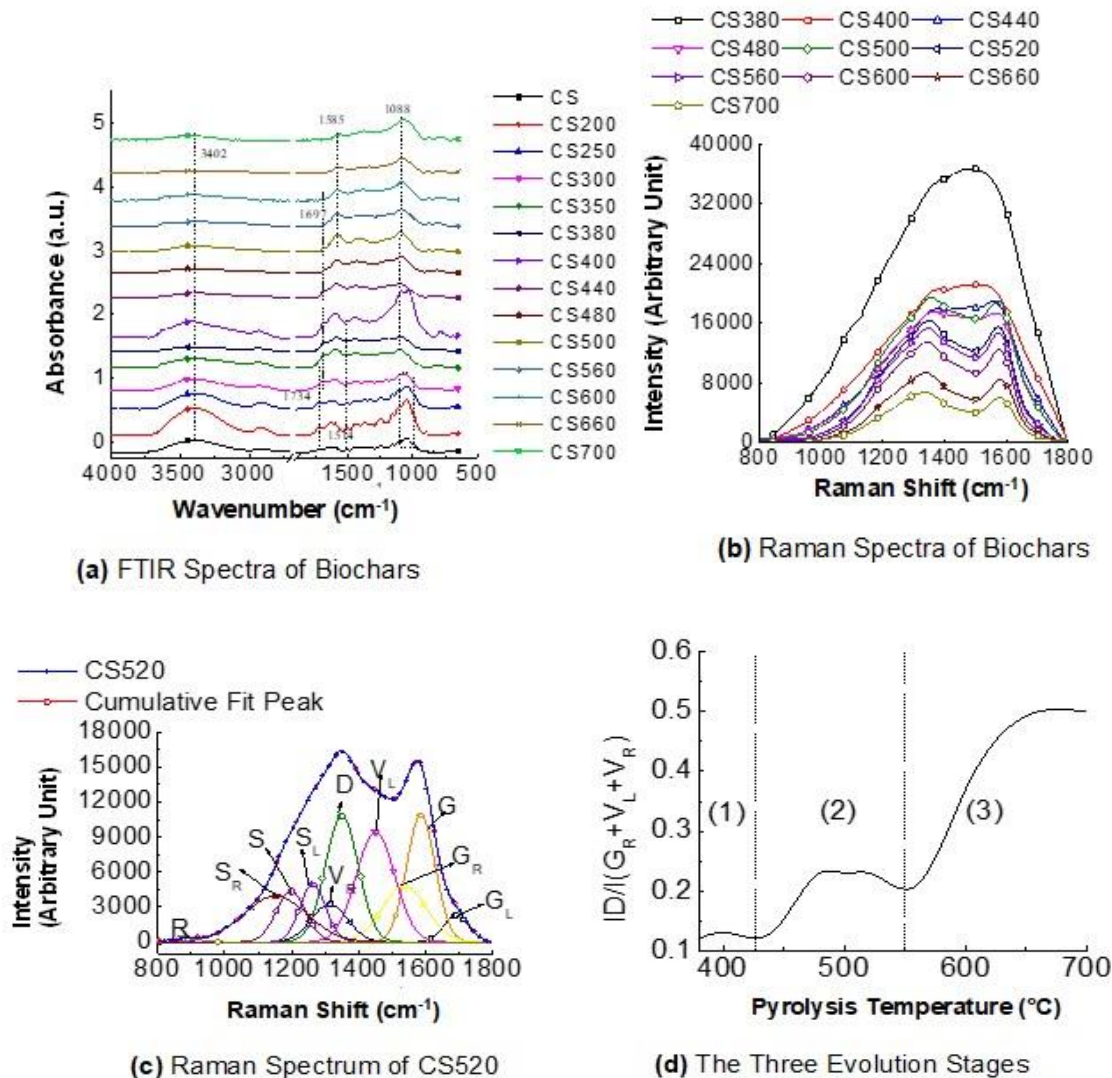


Fig. 7. FTIR (a), Raman (b) spectra of the biochar, the curve-fitting of a Raman spectrum of CS520 (c), and the three evolutionary stages during the carbonization of corn stover pellets (d)

Ultimate Analysis of Biochar

The ultimate composition of the biochar is presented in Table 2. With increasing temperature, the C and N contents in the biochar showed an increasing trend, while the H and O contents exhibited a downward trend, which could be attributed to the dehydration and decarboxylation reactions, resulting in decreases in the atomic ratios of H/C (from 1.50 to 0.30) and O/C (from 0.64 to 0.16).

The evolution of C, H, and O in the biochar followed the direction from the left and bottom in the Van-Krevelen diagram (Fig. 8a). The curve between O/C and H/C of the biochar can be expressed by $f(x)$, and $df(x)$ represents the relative loss rate ratio of H to O (Fig. 8a). H and O were lost in certain proportions before 320 °C, and H escaped greatly between 320 and 400 °C (Fig. 8a), because the volatile compounds after 320 °C mainly contained benzene compounds, phenols, and other H-rich compounds (Fig. 3). The relative loss rate ratio of H to O showed a rapid decline due to the release of polycyclic compounds, especially a large amount of methyl-substituted naphthalene from 440 to 520 °C (Fig. 6a). The loss rate of H increased suddenly between 560 and 700 °C, due to the release of PAHs and the gases including CO, CO₂, and H₂ (Fig. 8a), and dehydrogenation and polycondensation occurred mainly in the biochar, which was consistent with the value (Fig. 7d) and the detection of hydrogen (Fig. 2c). The H/C ratio, as an index, was calculated to evaluate the aromaticity and predict the aromatic cluster sizes of the biochar (Keiluweit *et al.* 2010; Xiao *et al.* 2016). For example, according to the model, between the size of the aromatic structures and the H/C ratio of the biochar (Xiao *et al.* 2016), the molecular structure of CS400 was predicted by using the H/C ratio, and CS400 had a H/C atomic ratio of 0.65. Hence, the aromatic cluster of CS400 was of a 2 × 2 rectangle distribution (Fig. 8a), which only represents the overall skeletal structure by taking biochar as a whole.

Table 2. Ultimate Analysis and Atomic Ratio of Biochar

Samples	Ultimate analysis			Atomic ratio	
	C(%)	H(%)	O(%)	H/C ^a	O/C ^a
CS200	44.43±0.04	5.54±0.05	37.98±0.24	1.50	0.64
CS250	48.62±0.06	5.31±0.01	35.37±0.14	1.31	0.55
CS280	50.69±0.46	5.09±0.12	32.84±0.82	1.21	0.49
CS320	60.75±0.38	4.32±0.11	22.7±0.51	0.85	0.28
CS380	61.32±0.02	3.82±0.05	22.06±0.34	0.75	0.27
CS400	60.53±0.36	3.3±0.02	21.19±0.38	0.65	0.26
CS440	63.69±0.22	3.06±0.03	17.74±0.42	0.58	0.21
CS480	64.31±0.08	2.9±0.02	17.01±0.01	0.54	0.2
CS500	64.44±0.07	2.67±0.07	16.78±0.17	0.50	0.2
CS520	65.29±0.02	2.44±0.05	16.02±0.08	0.45	0.18
CS560	65.8±0.33	2.28±0.19	15.27±0.52	0.42	0.17
CS600	65.74±0.22	2.06±0.06	14.55±0.61	0.38	0.17
CS660	65.8±0.41	1.95±0.09	14.22±0.45	0.36	0.16
CS700	65.11±1.15	1.61±0.27	13.64±1.66	0.30	0.16

^a H/C, atomic ratio of hydrogen to carbon. O/C, atomic ratio of oxygen to carbon

In order to explore the relationship between the release behavior of PAHs and the properties of biochar at different pyrolysis temperatures, the correlation between the H/C ratio of biochar and PAHs in the released products in the same period was analyzed (Fig. 8b). The relationship between the total amount of generated PAHs and H/C ratio of the

biochar at the same temperature could be fitted by a power function between 400 and 600 °C (Fig. 8b). The relationship between the total release amount of PAHs and the H/C ratio of biochar can help to predict the PAH release behavior of corn stover pellets in a certain temperature range from 400 to 600 °C. In this study, the released PAHs at each temperature were obtained in a narrow temperature range. Thus, the transient release amount of PAHs can be regarded as the release rate at each temperature during the whole pyrolysis process, and it is possible to obtain the approximate total release in a certain temperature range by integration. This correlation not only can explain the formation mechanism of PAHs at low temperature, but it also provides a theoretical basis for predicting the release of PAHs during the low-temperature corn stover pyrolysis process from 400 to 600 °C. However, when the pyrolysis temperature was above 600 °C, the H/C ratio of biochar was lower than 0.38, and the sum of the relative content of PAHs decreased. This result may be related to the carbon skeleton structure of larger size (>6-ring) due to the condensation of benzene ring in the biochar after 600 °C, which was consistent with the results of Raman analysis (Fig. 7c).

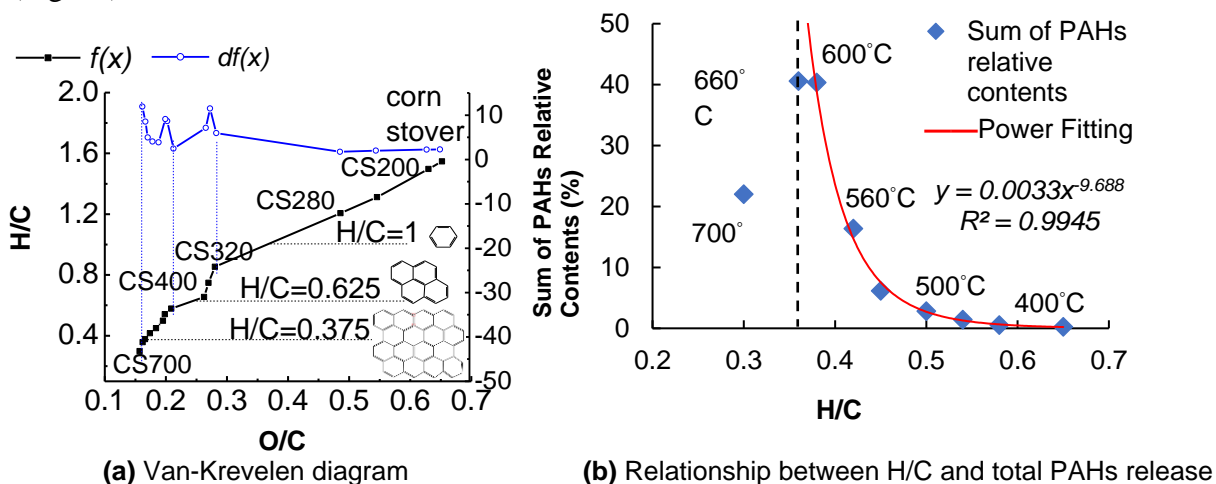


Fig. 8. Van-Krevelen diagram for corn stover pellet biochar (a) and the relationship between H/C ratio and total PAH release (b)

Reaction Pathway of PAHs during Corn Stover Pellet Pyrolysis

The formation and evolution of PAHs during corn stover pellet pyrolysis is shown in Fig. 9. In this study, the formation pathway of PAHs was deduced from the perspective of the pyrolysis products. The formation of PAHs in the pyrolysis process of corn stover pellets can be summarized as the following four pathways.

(1) Low-temperature PAH formation mechanism

Amorphous carbon structure just began to appear after the main components of corn stover pellets were decomposed from 380 to 440 °C; with increasing temperature, PAHs with low-order fused rings in the amorphous carbon structure were formed from 480 to 560 °C; then the carbon skeleton structure of larger size (>6-ring) due to condensation of benzene ring emerged and expanded from 600 to 700 °C; and the larger the aromatic system of the biochar was, the lower the release of PAHs would be (Figs. 7c and 9).

(2) *Naphthalene formation and growth pathway from phenols via cyclopentadienyl.* (Zhou *et al.* 2014)

Lignin (10.16% from Table 1) in corn stover pellets was decomposed to produce phenols, which can be converted into cyclopentadiene at high temperature; cyclopentene groups can be combined to form naphthalene, and they can also produce phenanthrene and other PAHs at high temperature.

(3) *The HACA process* (Zhao *et al.* 2020)

The presence of HACA in low temperature and pyrolysis needs to be further explored (Font Palma 2013). In this study, the HACA pathway is not the dominant pathway because of the low acetylene yield during the pyrolysis of corn stover pellets.

(4) *Methyl radical addition*

A large number of methyl radicals were contained in the gas phase products from the pyrolysis of corn stover pellets, and methyl radicals can form methyl derivatives of PAHs (Lee *et al.* 2008). The decomposition of partial methyl-substituted PAHs at high temperature would also contribute to the production of PAH monomers (Keiluweit *et al.* 2012; Zhou *et al.* 2014). The previous relevant results in this study (Figs. 2 to 8) showed that low-temperature PAH formation mechanism is the main reaction pathway during the pyrolysis of corn stover pellets, and phenol precursor pathway and methyl radical addition pathway serve as the auxiliary pathways. In addition, the HACA pathway may only play a minor role.

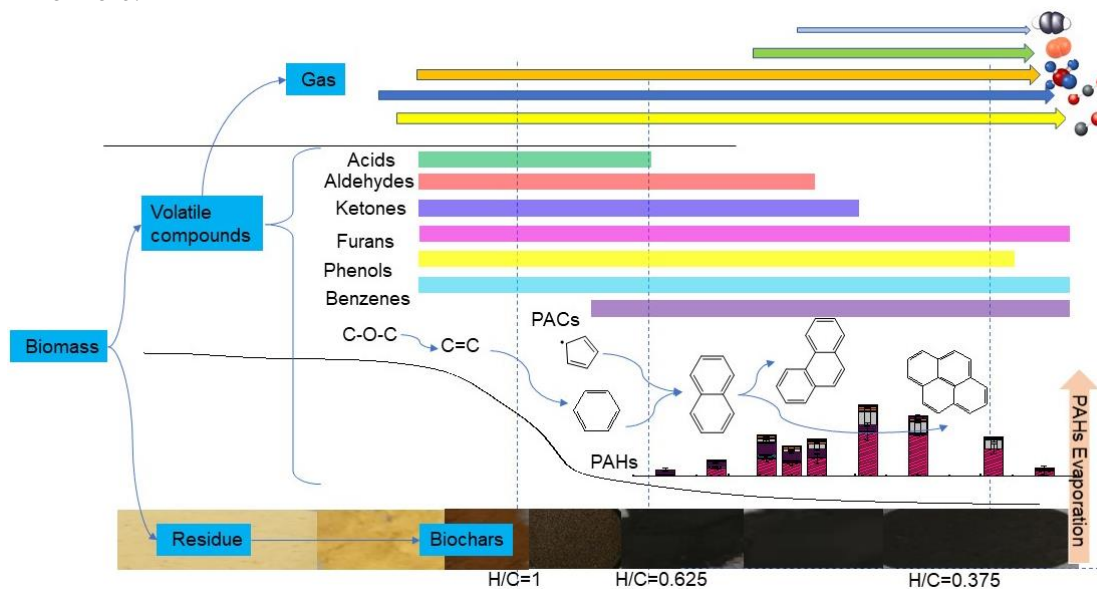


Fig. 9. Formation and evolution of PAHs during corn stover pellet pyrolysis

Combined with the negative pressure environment provided by the pyrolysis equipment in this study, during the heating process of corn stover pellets, the reactions such as depolymerization, decomposition, and bond breaking mainly occurred at the low temperature stage, resulting in the release of gaseous products that could quickly leave the reaction system. As a result, the secondary reaction of volatile matter was weakened, reducing the chance of PAH formation in the gas phase. Therefore, the detected production temperature of PAHs was higher than that detected in the literature (Sharma and Hajaligol

2003; Zhao *et al.* 2020). The dehydrogenation and polycondensation of biochar of corn stover pellets at the medium and high temperature stage formed different sizes of condensed ring carbon skeleton structures, which were cleaved and condensed to form a mixture of aromatic molecular clusters in the biochar at high temperature (in line with Gaussian distribution). After the connection between benzene rings in the biochar was broken, the 2 to 4 ring PAHs were released from the biochar and escaped under high temperature and negative pressure. In the industrial process of pyrolysis-based poly-generation systems of agricultural residues, positive measures can be taken to reduce the residence time of volatile compounds, control the evaporation and escape of PAHs at high temperature ($> 500\text{ }^{\circ}\text{C}$), and adjust the distribution of PAHs in the solid, liquid and gas products.

CONCLUSIONS

1. With the increase in temperature, a range of 2 to 4 ring PAHs in transient volatile compounds were analysed, including naphthalene, acenaphthylene, acenaphthene, fluorene, phenanthrene, anthracene, fluoranthene, and pyrene, and the release of these PAHs increased with increasing temperature from 400 to 560 $^{\circ}\text{C}$ with the peak at 560 $^{\circ}\text{C}$, and decreased from 560 to 700 $^{\circ}\text{C}$. The sum of relative content of these PAHs ranged from 0.23% to 40.36%. Besides, the derivatives of PAHs mainly included methyl, dimethyl- or trimethyl-naphthalene, methyl- or dimethyl-phenanthrene, hydrogenated naphthalene, and hydrogenated fluorene. However, the homologues and derivatives of acenaphthylene, acenaphthene, and fluoranthene were not detected.
2. The value $I_D / I_{(G_R+V_L+V_R)}$ of the biochar from 380 to 700 $^{\circ}\text{C}$ indicated a transition from preliminary formation of aromatic structure (380 to 480 $^{\circ}\text{C}$) to amorphous carbon structure (480 to 600 $^{\circ}\text{C}$), and further to the stage of dehydrogenation and the growth of aromatic rings (600 to 700 $^{\circ}\text{C}$) in the carbonization stage of corn stover pellets. It is worth noting that the relatively abundant amorphous carbon at around 560 $^{\circ}\text{C}$ contributed to the release of PAHs. The H/C ratio decreased continuously from 1.50 to 0.30 with the increase in pyrolysis temperature, suggesting that the aromaticity of the biochar increases with increasing pyrolysis temperature. The total amount of the generated PAHs and the H/C ratio of the biochar could be fitted by a power function (400 to 600 $^{\circ}\text{C}$), and the relation could be used to predict the potential of PAH release in pyrolysis-based poly-generation systems. The total amount of generated PAHs decreased at the temperature higher than 660 $^{\circ}\text{C}$.
3. Multiple pathways may occur separately to result in the formation of PAHs during the pyrolysis of corn stover pellets. Low-temperature PAH formation mechanism is the main reaction path in the slow pyrolysis of corn stover pellets, and the phenol precursor pathway and methyl radical addition pathway serve as the auxiliary pathways, while the HACA pathway only plays a minor role.

ACKNOWLEDGMENTS

This work was supported by the Agro–Scientific Research Project in the Public Interest [grant number 201503135]; the National Key Research and Development Project [Grant number 2019YFD1100501]; and the National Natural Science Foundation of China [grant number 31701310].

REFERENCES CITED

- ASTM D3174-2012. "Standard test method for ash in the analysis sample of coal and coke from coal," ASTM International, West Conshohocken, USA.
- ASTM D3175(2011). "Standard test method for volatile matter in the analysis sample of coal and coke," ASTM International, West Conshohocken, USA.
- ASTM D3302/D3302M (2015). "Standard test method for total moisture in coal," ASTM International, West Conshohocken, USA.
- Brewer, C. E., Schmidt-Rohr, K., Satrio, J. A., and Brown, R. C. J. (2009). "Characterization of biochar from fast pyrolysis and gasification systems," *Environmental Progress & Sustainable Energy* 28(3), 386-396. DOI: 10.1002/ep.10378
- Bucheli, T. D., Hilber, I., and Schmidt, H. (2015). "Polycyclic aromatic hydrocarbons and polychlorinated aromatic compounds in biochar," in: *Biochar for Environmental Management: Science, Technology and Implementation*, J. Lehmann and S. Joseph (eds.), Routledge, London, UK. DOI: 10.1088/0957-0233/12/7/328
- Buss, W., Graham, M. C., MacKinnon, G., and Mašek, O. (2016). "Strategies for producing biochars with minimum PAH contamination," *Journal of Analytical and Applied Pyrolysis* 119, 24-30. DOI: 10.1016/j.jaap.2016.04.001
- Chen, B., Zhou, D., and Zhu, L. J. (2008). "Transitional adsorption and partition of nonpolar and polar aromatic contaminants by biochars of pine needles with different pyrolytic temperatures," *Environmental Science & Technology* 42(14), 5137-5143. DOI: 10.1021/es8002684
- Cho, S.-H., Oh, J.-I., Jung, S., Park, Y.-K., Tsang, Y. F., Ok, Y. S., and Kwon, E. E. (2020). "Catalytic pyrolytic platform for scrap tires using CO₂ and steel slag," *Applied Energy* 259, article no. 114164. DOI: 10.1016/j.apenergy.2019.114164
- Cong, H., Masek, O., Zhao, L., Yao, Z., Meng, H., Hu, E., Ma, T. (2018). "Slow pyrolysis performance and energy balance of corn stover in continuous pyrolysis-based poly-generation systems," *Energy & Fuels* 32(3), 3743-3750. DOI: 10.1021/acs.energyfuels.7b03175
- Fagernäs, L., Kuoppala, E., and Simell, P. (2012). "Polycyclic aromatic hydrocarbons in birch wood slow pyrolysis products," *Energy & Fuels* 26(11), 6960-6970. DOI: 10.1021/ef3010515
- Font Palma, C. (2013). "Modelling of tar formation and evolution for biomass gasification: A review," *Applied Energy* 111, 129-141. DOI: 10.1016/j.apenergy.2013.04.082
- Friederici, L., Schneider, E., Burnens, G., Streibel, T., Giusti, P., Rüger, C. P., and Zimmermann, R. (2021). "Comprehensive chemical description of pyrolysis chars from low-density polyethylene by thermal analysis hyphenated to different mass spectrometric approaches," *Energy & Fuels* 35(22), 18185-18193. DOI:

- 10.1021/acs.energyfuels.1c01994
- Gelardi, D. L., Li, C., and Parikh, S. J. (2019). "An emerging environmental concern: Biochar-induced dust emissions and their potentially toxic properties," *Science of the Total Environment* 678, 813-820. DOI: 0.1016/j.scitotenv.2019.05.007
- Han, L., Nie, X., Wei, J., Gu, M., Wu, W., and Chen, M. (2021). "Effects of feedstock biopolymer compositions on the physiochemical characteristics of dissolved black carbon from lignocellulose-based biochar," *Science of the Total Environment* 751(2021), article no. 141491. DOI: 10.1016/j.scitotenv.2020.141491
- International Energy Agency (IEA) (2021). *Renewables 2021*, (<https://www.iea.org/reports/renewables-2021>), Paris, France.
- Keiluweit, M., Nico, P. S., Johnson, M. G., and Kleber, M. (2010). "Dynamic molecular structure of plant biomass-derived black carbon (biochar)," *Environmental Science & Technology* 44(4), 1247-1253. DOI: 10.1021/es9031419
- Keiluweit, M., Kleber, M., Sparrow, M. A., Simoneit, B. R., and Prah, F. G. (2012). "Solvent-extractable polycyclic aromatic hydrocarbons in biochar: Influence of pyrolysis temperature and feedstock," *Environmental Science & Technology* 46(17), 9333-41. DOI: 10.1021/es302125k
- Krzyszczak, A., Dybowski, M. P., and Czech, B. (2021). "Formation of polycyclic aromatic hydrocarbons and their derivatives in biochars: The effect of feedstock and pyrolysis conditions," *Journal of Analytical and Applied Pyrolysis* 160(2021), 105339. DOI: 10.1016/j.jaap.2021.105339
- Lee, J. G., Shin, E.-J., Pavelka, R. A., Kirchner, M. S., Dounas-Frazer, D., McCloskey, B. D., Petrick, D. E., McKinnon, J. T., and Herring, A. M. (2008). "Effect of metal doping on the initial pyrolysis chemistry of cellulose chars," *Energy & Fuels* 22(4), 2816-2825. DOI: 10.1021/ef700637s
- Legarra, M., Morgan, T., Turn, S., Wang, L., Skreiberg, Ø., and Antal, M. J. (2019). "Effect of processing conditions on the constant-volume carbonization of biomass," *Energy & Fuels* 33(3), 2219-2235. DOI: 10.1021/acs.energyfuels.8b03433
- Li, X., Hayashi, J., and Li, C. (2006). "FT-Raman spectroscopic study of the evolution of char structure during the pyrolysis of a Victorian brown coal," *Fuel* 85(12-13), 1700-1707. DOI: 10.1016/j.fuel.2006.03.008
- Li, Y., Liao, Y., He, Y., Xia, K., Qiao, S., and Zhang, Q. (2016). "Polycyclic aromatic hydrocarbons concentration in straw biochar with different particle size," *Procedia Environmental Sciences* 31, 91-97. DOI: 10.1016/j.proenv.2016.02.012
- Liu, J., Zhong, F., Niu, W., Su, J., Gao, Z., and Zhang, K. (2019). "Effects of heating rate and gas atmosphere on the pyrolysis and combustion characteristics of different crop residues and the kinetics analysis," *Energy* 175(15), 320-332. DOI: 10.1016/j.energy.2019.03.044
- Liu, W. J., Li, W. W., Jiang, H., and Yu, H. Q. (2017). "Fates of chemical elements in biomass during its pyrolysis," *Chemical Reviews* 117(9), 6367-6398. DOI: 10.1021/acs.chemrev.6b00647
- McGrath, T. E., Wooten, J. B., Geoffrey Chan, W., and Hajaligol, M. R. (2007). "Formation of polycyclic aromatic hydrocarbons from tobacco: The link between low temperature residual solid (char) and PAH formation," *Food and Chemical Toxicology* 45(6), 1039-50. DOI: 10.1016/j.fct.2006.12.010
- Muneer, B., Zeeshan, M., Qaisar, S., Razaq, M., and Iftikhar, H. (2019). "Influence of in-situ and ex-situ HZSM-5 catalyst on co-pyrolysis of corn stalk and polystyrene with a focus on liquid yield and quality," *Journal of Cleaner Production* 237, article

- no. 117762. DOI: 10.1016/j.jclepro.2019.117762
- Niu, W., Han, L., Liu, X., Huang, G., Chen, L., Xiao, W., and Yang, Z. (2016). "Twenty-two compositional characterizations and theoretical energy potentials of extensively diversified China's crop residues," *Energy* 100, 238-250. DOI: 10.1016/j.energy.2016.01.093
- Odinga, E. S., Gudda, F. O., Waigi, M. G., Wang, J., and Gao, Y. (2021). "Occurrence, formation and environmental fate of polycyclic aromatic hydrocarbons in biochars," *Fundamental Research*, 1(3), 296-305. DOI: 10.1016/j.fmre.2021.03.003
- Sharma, R. K., and Hajaligol, M. R. (2003). "Effect of pyrolysis conditions on the formation of polycyclic aromatic hydrocarbons (PAHs) from polyphenolic compounds," *Journal of Analytical and Applied Pyrolysis* 66(1-2), 123-144. DOI: 10.1016/s0165-2370(02)00109-2
- Sheng, C. (2007). "Char structure characterised by Raman spectroscopy and its correlations with combustion reactivity," *Fuel* 86(15), 2316-2324. DOI: 10.1016/j.fuel.2007.01.029
- Stark, A. K., and Ghoniem, A. F. (2017). "Quantification of the influence of particle diameter on polycyclic aromatic hydrocarbon (PAH) formation in fluidized bed biomass pyrolysis," *Fuel* 206, 276-288. DOI: 10.1016/j.fuel.2017.06.020
- Tsekos, C., Anastasakis, K., Schoenmakers, P. L., and de Jong, W. (2020). "PAH sampling and quantification from woody biomass fast pyrolysis in a pyroprobe reactor with a modified tar sampling system," *Journal of Analytical and Applied Pyrolysis* 147. DOI: 10.1016/j.jaap.2020.104802
- Wang, J., Odinga, E. S., Zhang, W., Zhou, X., Yang, B., Waigi, M. G., and Gao, Y. (2019). "Polyaromatic hydrocarbons in biochars and human health risks of food crops grown in biochar-amended soils: A synthesis study," *Environment International* 130, article no. 104899. DOI: 10.1016/j.envint.2019.06.009
- Wang, R., and Ben, H. (2020). "Accelerated aging process of bio-oil model compounds: A mechanism study," *Frontiers in Energy Research* 8(2020), 79. DOI: 10.3389/fenrg.2020.00079
- Weidemann, E., Buss, W., Edo, M., Masek, O., and Jansson, S. (2018). "Influence of pyrolysis temperature and production unit on formation of selected PAHs, oxy-PAHs, N-PACs, PCDDs, and PCDFs in biochar-a screening study," *Environmental Science and Pollution Research* 25(4), 3933-3940. DOI: 10.1007/s11356-017-0612-z
- Wong, J. W. C., Webber, J. B. W., and Ogbonnaya, U. O. (2019). "Characteristics of biochar porosity by NMR and study of ammonium ion adsorption," *Journal of Analytical and Applied Pyrolysis*, 143. DOI: 10.1016/j.jaap.2019.104687
- Xiao, X., Chen, Z., and Chen, B. (2016). "H/C atomic ratio as a smart linkage between pyrolytic temperatures, aromatic clusters and sorption properties of biochars derived from diverse precursory materials," *Scientific Reports* 6, article no. 22644. DOI: 10.1038/srep22644
- Xie, R., Zhu, Y., Zhang, H., Zhang, P., and Han, L. (2021). "Effects and mechanism of pyrolysis temperature on physicochemical properties of corn stalk pellet biochar based on combined characterization approach of microcomputed tomography and chemical analysis," *Bioresource Technology* 329, article no. 124907. DOI: 10.1016/j.biortech.2021.124907

- Xiong, Z., Guo, J., Chaiwat, W., Deng, W., Hu, X., Han, H., Chen, Y., Xu, K., Su, S., Hu, S., *et al.* (2020). "Assessing the chemical composition of heavy components in bio-oils from the pyrolysis of cellulose, hemicellulose and lignin at slow and fast heating rates," *Fuel Processing Technology* 199(2020), article no. 106299. DOI: 10.1016/j.fuproc.2019.106299
- Xiong, Z., Syed-Hassan, S., Hu, X., Guo, J., Qiu, J., Zhao, X., Su, S., Hu, S., Wang, Y., and Xiang, J. (2019). "Pyrolysis of the aromatic-poor and aromatic-rich fractions of bio-oil: Characterization of coke structure and elucidation of coke formation mechanism," *Applied Energy* 239(APR.1), 981-990. DOI: 10.1016/j.apenergy.2019.01.253
- Yan, R., Chen, H., Dong, H. L., and Zheng, C. (2007). "Characteristics of hemicellulose, cellulose and lignin pyrolysis," *Fuel* 86(12-13), 1781-1788. DOI: 10.1016/j.fuel.2006.12.013
- Yang, H., Dong, Z., Liu, B., Chen, Y., and Chen, H. (2020a). "A new insight of lignin pyrolysis mechanism based on functional group evolutions of solid char," *Fuel* 288, article no. 119719. DOI: 10.1016/j.fuel.2020.119719
- Yang, H., Gong, M., Hu, J., Liu, B., Chen, Y., Xiao, J., Li, S., Dong, Z., and Chen, H. (2020b). "Cellulose pyrolysis mechanism based on functional group evolutions by two-dimensional perturbation correlation infrared spectroscopy," *Energy & Fuels* 34(3), 3412-3421. DOI: 10.1021/acs.energyfuels.0c00134
- Yang, H., Li, S., Liu, B., Chen, Y., Xiao, J., Dong, Z., Gong, M., and Chen, H. (2020c). "Hemicellulose pyrolysis mechanism based on functional group evolutions by two-dimensional perturbation correlation infrared spectroscopy," *Fuel* 267, article no. 117302. DOI: 10.1016/j.fuel.2020.117302
- Yang, Q., Mašek, O., Zhao, L., Nan, H., Yu, S., Yin, J., Li, Z., and Cao, X. (2021). "Country-level potential of carbon sequestration and environmental benefits by utilizing crop residues for biochar implementation," *Applied Energy* 282, article no. 116275. DOI: 10.1016/j.apenergy.2020.116275
- Zhang, C., Shao, Y., Zhang, L., Zhang, S., Westerhof, R. J. M., Liu, Q., Jia, P., Li, Q., Wang, Y., and Hu, X. (2020). "Impacts of temperature on evolution of char structure during pyrolysis of lignin," *Science of the Total Environment* 699, article no. 134381. DOI: 10.1016/j.scitotenv.2019.134381
- Zhao, Y., Feng, D., Zhang, Y., Huang, Y., and Sun, S. (2016). "Effect of pyrolysis temperature on char structure and chemical speciation of alkali and alkaline earth metallic species in biochar," *Fuel Processing Technology* 141, 54-60. DOI: 10.1016/j.fuproc.2015.06.029
- Zhao, L., Zhao, Y., Nan, H., Yang, F., Qiu, H., Xu, X., and Cao, X. (2020). "Suppressed formation of polycyclic aromatic hydrocarbons (PAHs) during pyrolytic production of Fe-enriched composite biochar," *Journal of Hazardous Materials* 382, article no. 121033. DOI: 10.1016/j.jhazmat.2019.121033
- Zhou, H., Wu, C., Meng, A., Zhang, Y., and Williams, P. T. (2014a). "Effect of interactions of biomass constituents on polycyclic aromatic hydrocarbons (PAH) formation during fast pyrolysis," *Journal of Analytical and Applied Pyrolysis* 110, 264-269. DOI: 10.1016/j.jaap.2014.09.007
- Zhou, H., Wu, C., Onwudili, J. A., Meng, A., Zhang, Y., and Williams, P. T. (2014b). "Polycyclic aromatic hydrocarbon formation from the pyrolysis/gasification of lignin at different reaction conditions," *Energy & Fuels* 28(10), 6371-6379. DOI: 10.1021/ef5013769

Zhou, H., Wu, C., Onwudili, J. A., Meng, A., Zhang, Y., and Williams, P. T. (2015). "Polycyclic aromatic hydrocarbons (PAH) formation from the pyrolysis of different municipal solid waste fractions," *Waste Management* 36, 136-46. DOI: 10.1016/j.wasman.2014.09.014

Article submitted: January 20, 2022; Peer review completed: April 9, 2022; Revised version received: June 20, 2022; Accepted: August 9, 2022; Published: January 30, 2023. DOI: 10.15376/biores.18.1.2112-2136